Preparation and Alkali Metal Ion Exchange Properties of Protonated $Rb_8Nb_{22}O_{59}$ Compound

Xiaojing Yang,† Yoji Makita,* Junji Hosokawa, Kohji Sakane, and Kenta Ooi

National Institute of Advanced Industrial Science and Technology, 2217-14 Hayashi, Takamatsu 761-0395, Japan

Received April 20, 2005. Revised Manuscript Received August 24, 2005

An ion-exchanger $H_8Nb_{22}O_{59}\cdot 8H_2O$ was prepared by extracting Rb^+ from $Rb_8Nb_{22}O_{59}$, and its ion-sieve properties for alkali metal ions were investigated. The Rb^+ can be effectively extracted using a concentrated HNO_3 solution at room temperature, leading to a protonated compound with composition of $Rb_{0.14}H_{7.9}Nb_{22}O_{59}\cdot 8.2H_2O$. The protonated (hydronium ion form) crystal has the lattice parameters (a = 7.5104(2) and c = 43.0780(8) Å of hexagonal symmetry, $R\bar{3}m$), very close to the Rb^+-form precursor. The exchange capacity increased in the order $Cs^+ \ll Rb^+ < K^+$, $Na^+ < Li^+$, which agrees with the decreasing order of ionic radius. The capacities for Li^+, Na^+, and K^+ were close to the theoretical value of 2.55 mmol/g calculated from the composition of protonated compound. The distribution coefficients (K_d) of alkali metal ions were determined in the condition of microamount of ion loading. The selectivity sequence was Cs^+, $Li^+ \ll Na^+ < Rb^+ \ll K^+$ at pH around 3; the protonated samples showed markedly high selectivity for the adsorption of K^+. The pH titration curves showed a mono-base acid character toward Na^+, K^+, and Rb^+ ions. The analysis based on the ion-exchange model showed that it has a large amount of uniform acidic sites up to the neutralization degree of 0.5. The intrinsic acidities, pK_0 values, were evaluated as 1.6 for Na^+, K^+, and Rb^+ exchanges; this indicates that the ion-exchange sites have relatively strong acidity. The removal of Na^+ and K^+ impurities from Li^+-concentrated solutions was studied, and the removal rates for Na^+ and K^+ were found to reach 98 and 99.9%, respectively, from a solution containing 410 mM LiCl, 20 mM LiOH, 4.3 mM NaCl, and 1.0 mM KCl.

Introduction

One of the potential interesting features of metal oxide porous crystals (MOPCs) is their ion-exchange properties.[1,2] The ion-sieve type MOPCs are usually synthesized through the template method,[3] which can be divided into three stages: (1) inorganic compounds to be used as a matrix for the exchanger are mixed with template ions; (2) subsequently, the mixture is heated to form a precursor with the structure where each template ion is surrounded by matrix; and (3) template ions are topotactically removed to form porous crystals. This removal is generally carried out through acid treatment of precursors according to the ion-exchange reaction with protons. The extractability of the template ion is the important factor which determines the ion-exchange property of MOPC.

Since the extraction of template ions proceeds topotactically, maintaining the crystal structure of heat-treated precursor, MOPC, has pores or holes at the locations where the template ions have been removed. They show ion-sieve properties for the adsorption of cations, depending on the kind of template ions during the preparation. The ion-sieve properties of MOPCs can be characterized by distribution coefficient (K_d) measurement studies at a microamount of ion loading. Examples of ion-sieve type MOPCs with extremely high K_d values for certain metal ions have been summarized in the literature.[3,4] They can be successfully applied to the effective removal of minor ionic constituents from systems in which large amounts of similar kinds of cations coexist.[2,5]

We have proposed an "ion sieve radius" as a measure of pore size of MOPC since the size is too small to be evaluated using the conventional N_2 adsorption method.[6] Ion-sieve radius is defined as the radius of ion that shows the highest K_d value for metal ion exchange. For example, spinel-type manganese oxide has pores with ion-sieve radius (0.073 nm) corresponding to the ionic radius of Li^+, as it shows the highest K_d value for Li^+ among alkali metal ions. Scheme 1 summarizes some typical MOPCs with respect to the axis of ion-sieve radius.[6]

$Rb_8Nb_{22}O_{59}$ shows a unique ion-exchange behavior with smooth Rb^+/Na^+ and Rb^+/K^+ exchanges while no Rb^+/Li^+ exchange in an alkali metal chloride solution.[17] From its

* To whom correspondence should be addressed. Tel: +81-87-869-3511. Fax: +81-87-869-3550. E-mail: y-makita@aist.go.jp.

† Present address: Advanced Materials Laboratory, National Institute for Materials Science, Namiki 1-1, Tsukuba, Ibaraki 305-0044, Japan. Tel: +81-29-851-3354. Fax: +81-29-854-9061. E-mail: YANG.Xiaojing@nims.go.jp.

(1) (a) Clearfield, A. In *Inorganic Ion Exchange Materials*; CRC Press: Boca Raton, FL, 1982. (b) Clearfield, A. *Chem. Rev.* **1988**, *88*, 125.
(2) Paterson, R.; Rahman, H. *J. Colloid Interface Sci.* **1984**, *97*, 421.
(3) Feng, Q.; Kanoh, H.; Ooi, K. *J. Mater. Chem.* **1999**, *9*, 319.
(4) Abe, M. *Solvent Extr. Ion Exch.* **1995**, *12*, 381.
(5) Miyake, M.; Yoshida, T.; Uchida, H.; Ozawa, M.; Suzuki, T. *Chem. Mater.* **1991**, *3*, 572.
(6) Ooi, K. *J. Jpn. Ion-Exch. Soc.* **2001**, *12*, 47.
(7) (a) Ooi, K.; Miyai, Y.; Katoh, S.; Maeda, H.; Abe, M. *Langmuir* **1989**, *5*, 150. (b) Ooi, K.; Miyai, Y.; Katoh, S.; Maeda, H.; Abe, M. *Langmuir* **1990**, *6*, 289. (c) Ooi, K.; Miyai, Y.; Sakakibara, J. *Langmuir* **1991**, *7*, 1167. (d) Chitrakar R.; Kanoh H.; Miyai Y.; Ooi, K. *Chem. Mater.* **2000**, *12*, 3151.

10.1021/cm050835e CCC: $30.25
Published on Web 09/30/2005

Scheme 1. Some Typical Metal Oxide Porous Crystals Obtained via Template Method Plotted on the Axis of Ion Sieve Radius[a]

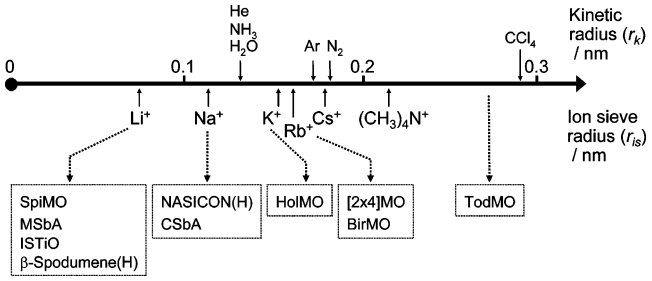

[a] r_{is} is the ion-sieve radius evaluated from the radius of the ion that shows the highest K_d value; r_k, kinetic radius calculated from the minimum cross-sectional diameter; SpiMO, spinel-type manganese oxide;[7] MSbA, monoclinic antimonic acid;[8] ISTiO, ion-sieve-type titanium oxide;[9] β-Spodumene(H), protonated spodumene;[10] NASICON(H), protonated super ionic conductor;[11] CSbA, cubic antimonic acid;[12] HolMO, hollandite-type manganese oxide;[13] [2×4]MO, manganese oxide with [2×4] tunnel structure;[14] BirMO, birnessite-type manganese oxide;[15] and TodMO, todorokite-type manganese oxide.[16]

unique ion-exchange behavior, we can expect a novel MOPC with niobium oxide framework when Rb^+ is removed from $Rb_8Nb_{22}O_{59}$. The synthesis and structure of $Rb_8Nb_{22}O_{59}$ were intensively studied in the 1960s to 1970s.[18−22] However, there have been few studies on the Rb^+ extraction behavior of $Rb_8Nb_{22}O_{59}$.

The present work describes the protonation of $Rb_8Nb_{22}O_{59}$ and the alkali metal ion-exchange properties of the protonated compound. A new kind of MOPC could be prepared by topotactic extraction of Rb^+ from $Rb_8Nb_{22}O_{59}$. The ion-sieve properties of the protonated material were studied by K_d measurement. Its ion-exchange properties from micro- to macroamount loading of alkali metal ions were studied by analysis of pH titration curves on the basis of ion-exchange model. From an applied standpoint, the removals of minor constituents K^+ and Na^+ from a concentrated LiCl solution were studied for purification of Li-base salt.

Experimental Section

Synthesis and Protonation of $Rb_8Nb_{22}O_{59}$. Rb_2CO_3 (0.755 g, Wako Chem. Co. Ltd., Japan) and Nb_2O_5 (0.2389 g, High Purity Chem. Co. Ltd., Japan) were mixed with distilled water (40 mL), and then the slurry was dried at 70 °C to vaporize water. The dried mixture was ground and put into a 50 mL alumina crucible and then heated at different temperatures from 700 to 1200 °C for 48 h. The powder samples were water-washed and dried at 70 °C overnight. *The samples obtained are named as Rn*, where *n* is from 7 to 12 corresponding to the heating temperature; e.g., R12 refers to the sample heated at 1200 °C.

The obtained sample (0.2 g) was treated with a 10 M HNO_3 solution (20 mL) for 3 days, then filtered, water-washed, and dried at 70 °C overnight. *The obtained samples are referred as to Rn-(H)*. For comparison, a corresponding sample was also treated with 1 M HCl in an autoclave at 90 °C for 2 days.

Composition Analysis. The solid sample (50 mg) was dissolved in a mixed solution of HF (5 mL) and HNO_3 (1 mL) while heating to 90−100 °C, after which 9 M H_2SO_4 (5 mL) was added. While still warm, the solution was put into a flask (100 mL) with oxalic acid (1 g) and water (30 mL). The rubidium and niobium contents in the solution were determined by inductively coupled plasma atomic emission spectrometry (ICP-AES) and the alkali metal contents by atomic absorption spectrophotometry (AAS). Note that we tried to use the alkali-melt method to dissolve the solid sample, but found that the melt produced with a mixture of Na_2CO_3 and H_3BO_3 could not dissolve in an HCl aqueous solution.

Ion-Exchange Capacity. The uptake of alkali metal ions from a mixed solution of 0.1 M XCl and 0.1 M XOH (X = Li, Na, K, Rb, and Cs) was carried out by intermittent shaking 50 mg of the protonated sample in a solution (5 mL) for 7 days at room temperature. The alkali metal ion concentration in the supernatant was determined by titration with 0.1 M HCl. The ion-exchange capacity was evaluated from the difference of the alkali metal concentration in the mother solution and in the supernatant solution. The values were confirmed by the analysis of the alkali metal content in solid products.

pH Titration Curve. A 40 mg portion of the protonated samples was immersed in a mixed solution (4 mL) of 0.1 M XCl and XOH (X = Li, Na, K, Rb, and Cs) in varying ratios. After intermittent shaking at room temperature for 7 days, the pH of the supernatant solution was determined. The solid samples after this experiment were separated by filtration. *They are referred as to Rn(X number)*, where X is the alkali metal ions used, and the number is the milimole of OH^- added in the solution (mmol/g of sample).

Distribution Coefficient (K_d). A 50 mg portion of R12(H) was immersed in 5 mL of a mixed solution of 1 mM XCl (X = Li, Na, K, Rb, and Cs) and shaken for 2 days. After the shaking, the metal ion concentrations in the supernatant solution were determined by AAS. The metal ion uptakes were calculated from the relative concentrations with the initial concentrations in the solution. The K_d values were calculated as

$$K_d\ (\mathrm{mL/g}) = \frac{\text{metal ion uptake (mmol/g)}}{\text{metal ion concentration after adsorption (mmol/ mL)}}$$

Removal of Minor Amounts of Potassium and Sodium Ions. Purification of lithium solution by removal of minor amounts of potassium and sodium ions was studied using two kinds of lithium-concentrated solutions (a solution containing 420 mM LiCl, 4.3 mM NaCl, and 1.0 mM KCl and that containing 410 mM LiCl, 20 mM LiOH, 4.3 mM NaCl, and 1.0 mM KCl) with different pH values. The R12(H) sample (100 mg) was shaken in each solution (10 mL) for 1 day and the concentration of each alkali ion in the supernatant solution was determined by AAS.

Instrumentation. X-ray diffraction (XRD) data were collected on a Rigaku RINT 2100 powder diffractometer using Cu Kα radiation. The XRD pattern for Rietveld refinement was measured

(8) (a) Chitrakar, R.; Abe, M. *Solvent Extr. Ion Exch.* **1989**, *7*, 725. (b) Chitrakar, R.; Abe, M. *Mater. Res. Bull.* **1988**, *23*, 1231.
(9) Onodera, H.; Iwasaki, T.; Hayashi, T.; Torii, K. *J. Ceram. Soc. Jpn.* **1989**, *97*, 888.
(10) Muller, G.; Hoffmann, M.; Neeff, R. *J. Mater. Sci.* **1988**, *23*, 1779.
(11) (a) Komorowski, P. G.; Argyropoulos, S. A.; Hancock, R. G. V.; Gulens, J.; Taylor, P.; Canaday, J. D.; Kuriakose, A. K.; Wheat, T. A.; Ahmad, A. *Solid State Ionics* **1991**, *48*, 295. (b) Makita, Y.; Ikai, O.; Sonoda, A. Hirotsu, T.; Ooi, K. *Proc. Int. Symp. Phys. Basis Adsorp.* (Okayama, Japan) **2000**, p 1P-4.
(12) Abe, M.; Ito, T. *Bull. Chem. Soc. Jpn.* **1967**, *40*, 1013. (b) Abe, M.; Ito, T. *Bull. Chem. Soc. Jpn.* **1969**, *42*, 2683.
(13) Tsuji, M.; Abe, M. *Solvent Extr. Ion Exch.* **1984**, *2*, 253.
(14) (a) Rziha, T.; Gies, H.; Rius, J. *Eur. J. Mineral* **1996**, *8*, 675. (b) Feng, Q.; Yokota, Y.; Makita, Y.; Yanagisawa, K.; Yamasaki, N. *High-Pressure Res.* **2001**, *20*, 33.
(15) Feng, Q.; Kanoh, H.; Miyai, Y.; Ooi, K. *Chem. Mater.* **1995**, *7*, 1226.
(16) Feng, Q.; Kanoh, H.; Miyai, Y.; Ooi, K. *Chem. Mater.* **1995**, *7*, 1722.
(17) Kumada, N.; Takagi, M.; Kinomura N. *Chem. Lett.* **1996**, 989.
(18) Reisman, A.; Holtzberg, F. *J. Phys. Chem.* **1960**, *64*, 748.
(19) Iyer, P. N.; Smith, A. J. *Acta Crystallogr.* **1971**, *B27*, 731.
(20) Gasperin, P. M. *Acta Crystallogr.* **1977**, *B33*, 398.
(21) Dewan, J. C.; Edwards, A. J.; Jones, G. R. *J. Chem. Soc. Dalton* **1978**, 968.
(22) Jones, G. R.; Robertson, D. S. *J. Cryst. Growth* **1978**, *43*, 115.

Table 1. Analyzed Composition of the As-prepared Samples and the Rb Extraction Rate by Acid Treatment

	metal content			extraction by HNO_3		extraction by HCl	
sample no.	Rb/mmol g^{-1}	Nb/mmol g^{-1}	Rb/Nb	Rb/mmol g^{-1}	extraction rate	Rb/mmol g^{-1}	extraction rate
R7	2.14	6.19	7.59/22	2.10	0.981	1.82	0.851
R8				2.18		1.83	
R9	2.21	6.33	7.69/22	2.21	1.000	1.89	0.854
R10				2.22		1.78	
R11				2.13		1.61	
R12	2.23	6.09	8.04/22	2.18	0.978	1.71	0.768
R12(H)	0.045	6.86	0.14/22				

by the fixed time method, accumulation time (6 s) for each 2θ point. The Rietveld refinement was performed using the software of RIETAN-2000.[23] The lattice constant was also calculated from d values by the use of the procedure Cell Refinement in the software of Jade 5 (Materials Data, Inc.). Thermogravimetric and differential thermal analysis (TG-DTA) curves were obtained on a MAC SCIENCE type 2000 thermal analyzer at a heating rate of 10 K min^{-1} in air. Scanning electron microscope (SEM) images were taken on a Hitachi S-2460N.

Results and Discussion

Preparation and Characterization of Protonated $Rb_8Nb_{22}O_{59}$. The XRD patterns of the rubidium niobium oxides obtained at different temperatures are shown in Figure 1. The crystallinity increases with an increase in the heating

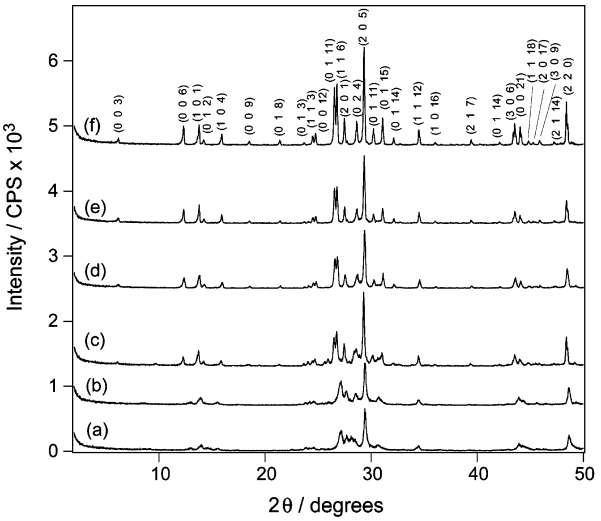

Figure 1. XRD patterns for the samples heated at (a) 700, (b) 800, (c) 900, (d) 1000, (e) 1100, and (f) 1200 °C for 2 days.

temperature. The Rb/Nb molar ratio determined by chemical analysis also increases with heating temperature (Table 1). The composition of R12 can be written as $Rb_{8.04}Nb_{22}O_{59.01}$, which is close to the theoretical composition of $Rb_8Nb_{22}O_{59}$. All peaks in the XRD pattern of R12 can be indexed to hexagonal symmetry (Figure 1f), corresponding to JCPDS card No. 34-1019. The lattice parameters ($a = 7.51$ and $c = 43.12$ Å) calculated are close to those (7.511(1) and 43.13-(1) Å) prepared by Kumada et al.[17] at 900 °C using a similar method and those of a single crystal by Jones and Robertson (7.52 and 43.17 Å),[22] but are slightly smaller than those reported by Dewan et al. (7.53(1) and 43.39(6) Å).[21]

(23) (a) Izumi, F.; Ikeda, T. *Mater. Sci. Forum* **2000**, *321−324*, 198. (b) Homepage of Izumi, F. http://homepage.mac.com/fujioizumi/.

The acid treatment of the samples with 10 M HNO_3 for 3 days resulted in the extraction of more than 97% of Rb ions from the solids (Table 1). The amount of niobium ions dissolved in the supernatant solution was very small (0.02−0.04%), indicating that the niobium oxide is stable enough in such a highly concentrated HNO_3 solution. The extraction rate is higher in the HNO_3 solution than in a 1 M HCl solution at 90 °C. The XRD analysis shows that the Rb^+ extraction does not show remarkable changes in peak position nor does it produce new phase peaks, but only undergoes changes of relative intensities of the peaks, for example, of the peaks at 2θ around 24.5° and around 39.5° (Figure 2).

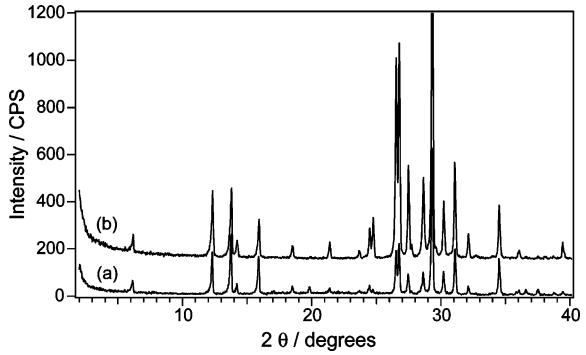

Figure 2. XRD pattern of (a) the R12 (H) sample compared with (b) as-prepared R12.

The SEM images of R12 and R12(H) do not show noticeable morphology change (Figure 3), indicating the topotactic extraction of Rb^+.

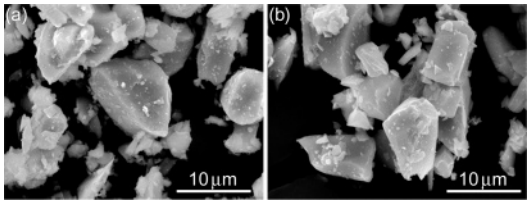

Figure 3. SEM images of (a) as-prepared R12 and (b) R12 (H).

These results indicate that well-crystallized $Rb_8Nb_{22}O_{59}$ can be obtained at high temperature, and the concentrated HNO_3 solution is effective for the extraction of Rb^+ from the solid.

Figure 4 gives the TG-DTA curves for R12 and R12(H). The R12 sample does not show any peaks in the DTA curve since $Rb_8Nb_{22}O_{59}$ has a high melting point of 1420 °C.[21] In contrast, the R12(H) sample shows an endothermic peak at 385 °C followed by an exothermic one at 430 °C in the DTA curve. The TG curve indicates the first large weight loss of 4.69% between room temperature and 385 °C, although DTA peaks are not observed in this region. The second weight

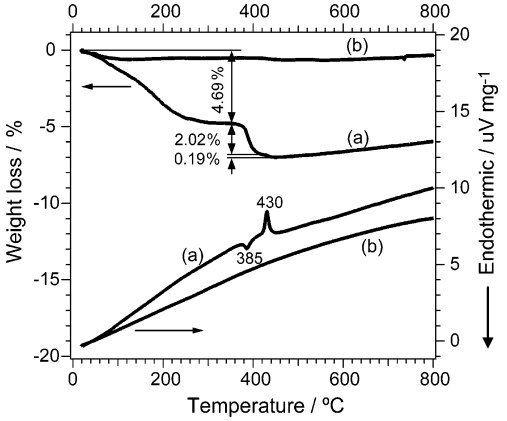

Figure 4. TG-DTA curves of the R12 sample (a) protonated in HNO_3 and (b) as-prepared.

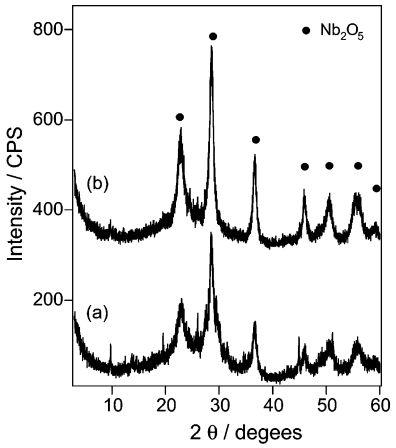

Figure 5. XRD patterns of the protonated sample heated at (a) 250 and (b) 450 °C for 2 h.

loss of 2.02% corresponding to the 385 °C endothermic peak and the third weight loss of 0.19% corresponding to the exothermic peak appear in the TG curve. The XRD patterns of the products after the R12(H) sample was heated at 250 and 450 °C, respectively, are given in Figure 5. The pattern after 250 °C heating shows the peaks corresponding to niobium pentaoxide (Nb_2O_5)[24] with relatively broad character and sharp peaks at $2\theta = 9.7$, 19.6, 26.3, 29.5, and 22.9°. The sharp peaks can be indexed to the $Rb_{0.125}Nb_{0.375}O$ or $Rb_{7.3}Nb_{22}O_{58.7}$ phase,[25] but it may be a protonated phase because R12(H) has a very low Rb/Nb ratio of 0.14/22 (Table 1) and furthermore the decrease in intensity of the sharp peaks exhibits the phase changes to Nb_2O_5 after heating at 450 °C (Figure 5b). Thus, the weight losses can be characterized due to the evaporation of lattice water between 60 and 300 °C and the release of lattice proton with oxygen between 300 and 450 °C.

According to the Rb and Nb contents (Table 1) and H_2O and H^+ contents (the TG-DTA result), the composition of R12(H) could be calculated as $Rb_{0.14}H_{7.9}Nb_{22}O_{59}\cdot 8.2H_2O$. It is noticeable that the water content is close to the proton content. Considering that the temperature (around 150 °C) of water evaporation is relatively higher than that for conventional water evaporation, we can conclude that the protons are in the form of hydronium ions (H_3O^+) in a niobium oxide lattice. Namely, the Rb^+ extraction proceeds through an H_3O^+/Rb^+ ion-exchange reaction.

(24) JCPDS No. 28-0317.
(25) JCPDS No. 34-0846.

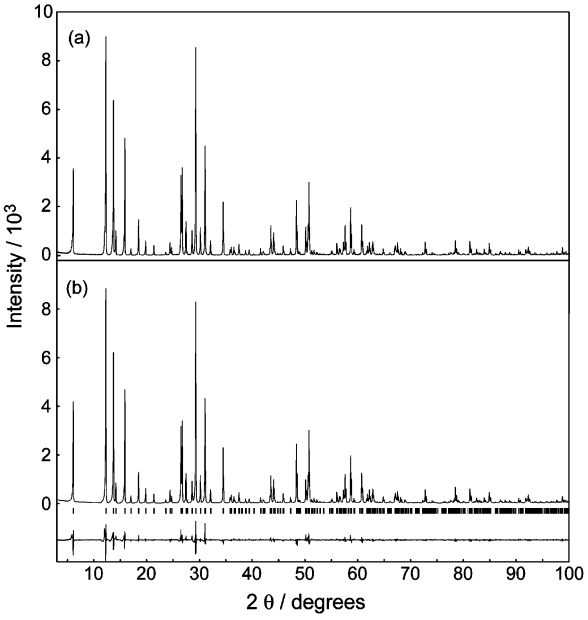

Figure 6. Plots of Rietveld refinement for R12(H). Above are the observed (a) and simulated (b) intensity data (I_o and I_s), respectively. Below is their deviance ($I_o - I_s$). The tick marks indicate the positions of all possible Bragg reflections.

Table 2. Final Atomic Positional Parameters and Lattice Parameters Obtained by Rietveld Refinement for R12(H)[a]

lattice parameters/Å	unit-cell volume/Å^3
$a = 7.5104(2)$[b] $c = 43.0780(8)$	2104.31(9)

atom	position	x	y	z	B/Å^2
Nb(1)	18h	0.1684(2)	0.3369	0.0298(0)	1.2(0)
Nb(2)	6c	0	0	0.0963(1)	1.9(0)
Nb(3)	9d	$^1/_3$	$^1/_6$	0.1698(2)	1.1(1)
O(1)	18h	0.1244(9)	0.2488	0.0711(2)	4.2(4)
O(2)	18h	0.2412(18)	0.1206	0.1251(2)	4.0(5)
O(3)	18h	0.2975(17)	0.1488	0.0189(3)	1.1(3)
O(4)	18h	0.4499(8)	0.8999	0.0325(2)	2.6(4)
O(5)	18h	0.1255(7)	0.2509	0.1738(3)	1.3(4)
WO(1)[c]	6c	$^2/_3$	$^1/_3$	0.0809(6)	10.6(7)
WO(2)	6c	$^1/_3$	$^2/_3$	0.1235(5)	$=B$(WO(1))

[a] Space group $R\bar{3}m$ (No. 166). Reliability factors: $R_{wp} = 0.1413$, $R_p = 0.1030$, $R_R = 0.1314$, $R_e = 0.0788$; goodness-of-fit indicator $S = 1.7931$; and Durbin-Watson statistic: d1 = 0.8489, d2 = 0.9421. [b] Estimated standard deviations in parentheses. [c] Virtual chemical species WO = H_3O.

The presence of lattice H_3O^+ is also supported by a Rietveld refinement of the XRD pattern of R12(H). As shown in Figure 6 and Table 2, all the simulated peaks coincide well with the observed ones and the reliability factors are satisfactory. The stoichiometry of the compound $(H_3O)_8Nb_{22}O_{59}$ was employed in the crystal-structure analysis, when introducing a virtual chemical species WO whose atomic scattering factor was set equal to the sums of those of one O and three H atoms. The unit cell contents corresponded to $(H_3O)_{12}Nb_{33}O_{90}$, and as indicated by Dewan et al. for the structure analysis of $Rb_8Nb_{22}O_{59}$,[21] a disordered vacancy in one of the oxygen positions was assumed but not defined. There was no evidence of refinement improvement if the small amount of Rb ions residual in R12(H) was considered.

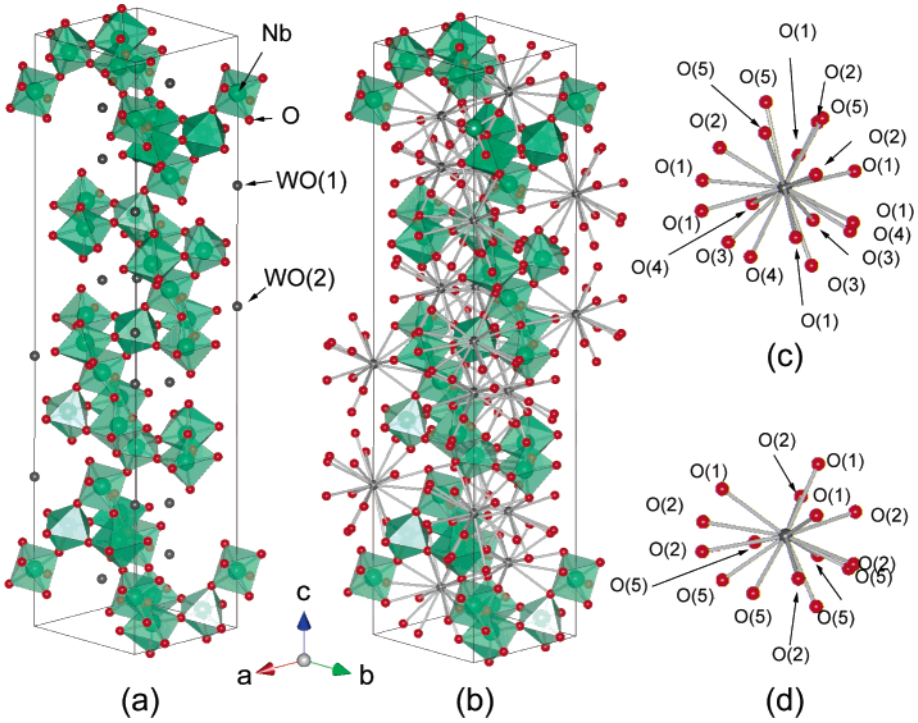

Figure 7. Structure models based on the Rietveld refinement, showing (a) the octahedral coordination of niobium atoms by oxygen, and (b) the coordination of the H_3O^+ ions, for whose two kinds of sites, WO(1) and WO(2), the magnifications are shown in (c) and (d), respectively. The straight black outline indicates the unit cell.

Table 3. Selected Interatomic Distances with Estimated Standard Deviations in Parentheses

Nb atoms	distances/Å	WO (1) atoms[a]	distances/Å	WO (2) atoms	distances/Å
Nb(1)−O(1)	1.868(10)	WO(1)···O(1)	3.81806(10)	WO(2)···O(1)	3.53166(6)
Nb(1)−O(4)	1.914(3)		3.81806(10)		3.53216(4)
Nb(1)−O(3)	2.117(11)		3.81880(9)		3.53216(6)
Nb(1)−O(3)	2.127(5)		3.81880(10)	WO(2)···O(2)	3.80296(10)
Nb(2)−O(1)	1.948(11)		3.81853(3)		3.80296(10)
Nb(2)−O(2)	2.002(10)		3.81853(6)		3.80370(9)
Nb(3)−O(2)	1.761(12)	WO(1)···O(2)	3.36047(6)		3.80343(3)
Nb(3)−O(5)	1.963(3)		3.36100(3)		3.80343(7)
Nb(3)−O(5)	1.964(3)		3.36100(6)		3.80370(10)
Nb(3)−O(5)	2.005(4)	WO(1)···O(3)	3.58800(5)	WO(2)···O(5)	3.46724(6)
Nb(3)−O(5)	2.006(4)		3.58843(4)		3.11816(3)
Nb(3)−O(2)	2.013(13)		3.58843(5)		3.11816(6)
		WO(1)···O(4)	3.50513(6)		3.11861(6)
			3.50513(3)		3.46775(3)
			3.50565(6)		3.46775(6)
		WO(1)···O(5)	3.76020(5)		
			3.76020(5)		
			3.76045(6)		

[a] Volumes of the polyhedrons are 136.3788 and 106.2209 Å^3 for WO(1) and WO(2), respectively.

The crystal-structure model of $(H_3O)_8Nb_{22}O_{59}$ is given in Figure 7 according to the refinement result. The Nb atoms are in a distorted octahedral site coordinated by oxygen. The Nb−O distances range between 1.868 and 2.127 Å (Table 3), which are close to the values[18] (from 1.842 to 2.138 Å) in Rb form [$Nb_{22}O_{59}$]. This means that the H_3O^+/Rb^+ ion exchange rarely influences the structure of Nb−O framework and the ion-exchange reaction progresses topotactically. We can distinguish two kinds of H_3O^+ sites, WO(1) and WO(2), in the protonated sample. WO(1) has 18 oxygen atom neighbors (Figure 7c) with WO···O distances ranging from 3.50 to 3.82 Å (average 3.54 Å), whereas the WO(2) site has 15 oxygen atom neighbors with WO···O distances ranging between 3.12 and 3.80 Å (average 3.64 Å) (Figure 7d), which is close to the Rb···O distances in the Rb form,[21] where the Rb−O distance ranges from 3.24 to 3.81 Å. Consequently, half of the hydronium ions locate in the WO(1) site with larger pore size and another half in the WO(2) site with smaller pore size. The volume difference of the pores is as large as ca. 22%, which is shown by the volumes of oxygen polyhedrons (Table 3).

Ion-Exchange Capacity. Ion-exchange capacities of the protonated samples for alkali metal ions were determined from mixed solutions of XCl and XOH (X = Li, Na, K, Rb, and Cs), as summarized in Table 4. The protonated samples heated at 700, 900, and 1200 °C showed a similar tendency of ion-exchange capacity in the mixed solution. The exchange capacity increases in the order $Cs^+ \ll Rb^+ < K^+, Na^+ < Li^+$, which agrees with the decreasing order of ionic radius. The capacities for Li^+, Na^+, and K^+ are close to the theoretical value of 2.55 mmol/g calculated from the composition of $(H_3O)_8Nb_{22}O_{59}$. All the samples barely adsorb

Table 4. Adsorptive Capacity of Protonated Samples[a]

	uptake amount/mmol g^{-1}				
sample	Li^+	Na^+	K^+	Rb^+	Cs^+
R7(H)	2.49	2.21	2.28	1.70	0.19
R9(H)	2.45	2.23	2.29	1.55	0.17
R12(H)	2.99	2.86	2.55	2.15	0.12

[a] Solid: 50 mg. Solution: a mixed solution of 0.1 M metal chloride and 0.1 M metal hydroxide, 5 mL.

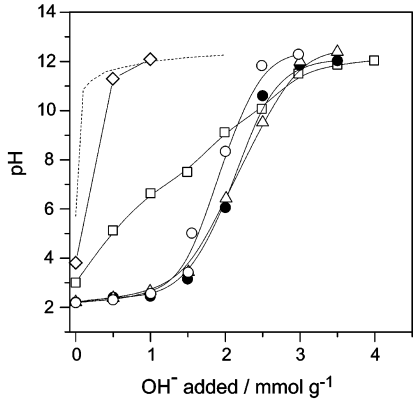

Figure 8. pH titration curves of the protonated R12 sample: (□) Li^+; (●) Na^+; (△) K^+; (○) Rb^+; (◇) Cs^+; dotted line, blank.

Cs^+; it may be too large to enter the ion-exchange sites in the crystal lattice. The alkali metal ion-exchange properties of protonated $Rb_8Nb_{22}O_{59}$ are different from those of $Rb_8Nb_{22}O_{59}$ reported by Kumada et al.,[17] in which K^+ and Na^+ exchange smoothly with Rb^+ in the solid, but Li^+ rarely exchanges. Since the sites have a higher affinity for Rb^+ than Li^+ (to be shown below), Li^+ may not be exchangeable with Rb^+ ions of $Rb_8Nb_{22}O_{59}$.

pH Titration Study. The pH titration curves of R12(H) toward alkali metal ions are given in Figure 8. In coincidence with the small uptake of Cs^+ in the capacity study (Table 4), the curve toward Cs^+ is close to the blank titration curve. This suggests that Cs^+ rarely exchanges with the lattice protons, but only with the hydroxyl group at the surface of the metal oxide. The apparent adsorptive capacity, evaluated from the amount of OH^- added, increases in the order $Cs^+ \ll Li^+ \ll Na^+$, K^+, Rb^+ at pH 4. The order of the apparent capacity changes to $Li^+ < Rb^+ < Na^+$, K^+ at pH between 4 and 8 and the apparent capacity for Li^+ becomes the largest at pH above 11. This shows that the site has low affinity for Li^+ but the largest capacity.

Some thermodynamic parameters can be derived from a pH titration curve, as is described in our previous study.[7] The ion-exchange reaction can be written as

$$H^+(s) + M^+(l) \leftrightarrow H^+(l) + M^+(s) \quad (1)$$

where $H^+(s)$ and $M^+(s)$ are species in solid phase and $H^+(l)$ and $M^+(l)$ are those in liquid phase. The selectivity coefficient K_c can be evaluated from the pH titration as follows

$$pK_c = -\log K_c \leftrightarrow pH - \log[\alpha/(1-\alpha)] + \log C_M \quad (2)$$

where α is the degree of exchange, which corresponds to the equivalent fraction of exchanged M^+ in the solid phase. C_M is the concentration of alkali metal ions in the liquid phase. The α value can be calculated as $\alpha = A/A_{max}$, where

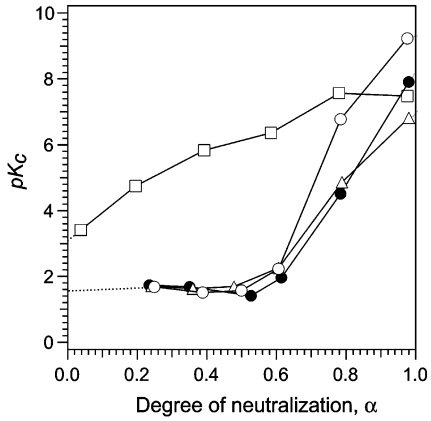

Figure 9. pK_c vs degree of neutralization plots calculated from Figure. 8. (□) Li^+; (●) Na^+; (△) K^+; (○) Rb^+.

Table 5. Values of pK_0, pK, and $\Delta G°$ (Temperature 296 K) for the R12(H) Sample

	pK_0	pK	$\Delta G°/10^3$ J mol^{-1}
Li^+/H^+	3.1	6.0	34.0
Na^+/H^+	1.6	2.9	16.4
K^+/H^+	1.6	3.0	16.7
Rb^+/H^+	1.6	3.6	20.2

A is the metal ion uptake (mmol/g) and A_{max} is the maximum metal ion uptake (mmol/g), corresponding to the ion-exchange capacity. The stability constant K of eq 1 and the standard Gibbs free energy ($\Delta G°$) can be evaluated by using the simplified treatment of the Gain-Thomas equation,[26]

$$pK = -\log K = \int_0^1 pK_c \, d\alpha \quad (3)$$

$$\Delta G° = (2.303RT)pK \quad (4)$$

The selectivity coefficient pK_c for alkali metal ions can be calculated from the data in Figure 8. Because the alkali metal ion exchange takes place even from alkali metal chloride solution on the protonated sample, the metal ion uptake could not be calculated only from the amount of OH^- added as in the previous papers.[26,27] The metal ion uptake, A (mmol/g), was calculated according to the formula $A = ([OH^-]_0 + [H^+])V/m$, where $[OH^-]$ is the initial OH^- concentration (mM), $[H^+]$ the equilibrium concentration (mM) of H^+ determined by pH measurement, V the volume of solution, and m the amount of the protonated sample added (g).

The calculated pK_c values versus the degree of exchange, α, are shown in Figure 9. The thermodynamic equilibrium constant (K) and standard Gibbs free energy change ($\Delta G°$) for each M^+/H^+ ion exchange are summarized in Table 5. The intrinsic selectivity coefficient pK_0 was derived by extrapolating α in Figure 9 to zero. The pK_0 value on "zero loading" of the ion-exchange reaction reflects the intrinsic acidity of the site at the hypothetical ion exchange between the isolated site and an ion. The R12(H) sample has the same pK_0 of 1.6 for Na^+, K^+, and Rb^+ ions. The pK_0 values smaller than that ($pK_0 \approx 4$) of the conventional carboxylate-type resin mean that the ion-exchange sites have relatively

(26) Gaines, G. L. Jr.; Thomas, H. C. *J. Chem. Phys.* **1953**, *21*, 714.
(27) (a) Ooi, K.; Miyai, Y.; Katoh, S.; Maeda H.; Abe, M. *Bull. Chem. Soc. Jpn.* **1988**, *61*, 407. (b) Ooi, K.; Abe, M. *Solvent Extr. Ion Exch.* **1996**, *16*, 1137.

Table 6. Lattice Parameters of Alkali Metal Inserted Samples after pH-titration

sample	*a*/Å	*c*/Å	volume/Å^3
R12(H)	7.51	43.12	2106
R12(Li-3.5)	7.54	43.13	2124
R12(Na-3.5)	7.48	43.57	2111
R12(K-0)	7.56	43.36	2146
R12(K-3.5)	7.56	43.60	2158
R12(Rb-0)	7.53	43.14	2118
R12(Rb-3)	7.52	43.15	2113
R12(Cs-1)	7.51	43.11	2106

strong acidity. Compared with Na^+, K^+, and Rb^+ ions, the higher pK_0 value (3.1) for Li^+/H^+ exchange indicates that Li^+ is less exchangeable with the lattice protons in the isolated condition. Since hydrated Li^+ has the largest size among the hydrated alkali metal ions, it must be dehydrated to the largest extent in order to enter the crystal lattice. The requirement of larger dehydration energy may cause the higher pK_0 value for Li^+.

The pK_c values for Na^+, K^+, and Rb^+ are nearly constant in the region below 0.5, while they increase steeply with α in the region $\alpha > 0.5$. This shows that the metal ions become less exchangeable with α in the region $\alpha > 0.5$. The pK_c curves suggest the presence of two kinds of ion-exchange sites: the site independent of exchanged metal ions and that dependent on exchanged metal ions. The presence of two kinds of exchange site relates well to the results of the X-ray diffraction study, where the protonated sample has two kinds of exchangeable lattice protons, WO(1) and WO(2).

Structural Change during M^+/H^+ Ion Exchange. The XRD analyses were carried out for the samples after the pH titration; for all the samples the peaks from $2\theta = 3$ to 70° can be indexed to the same symmetry as R12(H). Magnifications of the (006) and (101) peaks for the entire exchanged samples are given in Figure 10. The lattice parameter *a* (= *b*) and *c* given in Table 6 can be evaluated according to the relation of $1/d^2 = 4/3(h^2 + hk + k^2)/a^2 + l^2/c^2$ for hexagonal symmetry as follows

$$6d_{(006)} = c \tag{5}$$

$$d_{(101)}{}^{-2} = \frac{4}{3}a^{-2} + c^{-2} \tag{6}$$

The high-magnification XRD analyses clearly show that the diffraction peaks do not shift by the Cs^+ or Rb^+ loading (Figure 10). The constant *a* and *c* parameters for the Cs^+-loaded samples supports the above conclusion that Cs^+ cannot enter the crystal lattice, but is adsorbed only at the surface of the crystal. In the case of Li^+, Na^+, and K^+ ion exchanges, the diffraction peaks shift slightly with the amount of alkali metal ion loading in the region $\alpha > 0.6$. The Li^+ loading results in the expansion of lattice *a* (and *b*), the Na^+ loading the expansion of lattice *c* as well as the shrinking lattice *a* (and *b*), and the K^+ loading causing a slight expansion of lattice *c* parameter. The change in lattice parameter in the region of high metal ion loading suggests that the alkali metal ion-exchange reactions are influenced slightly by the exchanged metal ions in the region of high metal ion loading.

Distribution Coefficient (K_d). The distribution coefficients of alkali metal ions were determined in the condition of microamount ion exchange, as shown in Table 7. The selectivity sequence is Cs^+, $Li^+ \ll Na^+ < Rb^+ \ll K^+$ at pH around 3; the protonated samples show markedly high selectivity for the adsorption of K^+, independent of preparation temperature. A similar selectivity sequence has been observed on hollandite-type manganese oxide with [2 × 2] tunnels,[13] which is suitable for the stable fixing of K^+. The present protonated sample may have ion-exchange sites with pore size suitable for fixing K^+ ions.

The selectivity sequence changes to $Cs^+ < Na^+ \ll Rb^+ < K^+ \ll Li^+$ at pH around 7, where a markedly high selectivity for Li^+ has been observed. Since the lattice protons are easily dissociated at high pH, the electrostatic interaction between alkali metal ions and anionic ion-exchange site may become important. Since Li^+ has the smallest ionic size, the strong electrostatic attraction between ion-exchange site

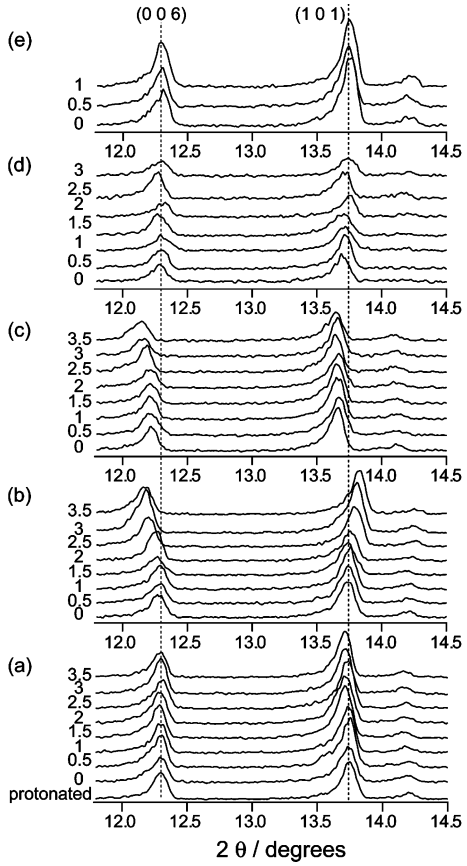

Figure 10. Changes of (006) and (101) plane XRD peaks after different amounts of (a) Li^+, (b) Na^+, (c) K^+, (d) Rb^+, and (e) Cs^+ ions exchanged with proton. The number indicates the amount of OH^- added (mmol/g), as shown in Figure 8.

Table 7. Alkali Metal Ion Distribution Coefficient K_d for the Protonated Samples

sample	solution[a]	K_d/mL g^{-1} Li	Na	K	Rb	Cs	pH after adsorption
R12(H)	A	<10	580	18000	1200	<10	3.04
R11(H)	A	<10	590	32000	1000	10	
R9(H)	A	<10	220	28000	1400	34	
R8(H)	A	<10	410	15000	740	53	
R7(H)	A	<10	310	13000	420	220	
R12(H)	B	>50000	1300	14000	13000	120	7.32

[a] A: 1 mM LiOH + 1 mM NaOH + 1 mM KOH + 1 mM RbCl + 1 mM CsCl. B: 1 mM LiOH + 1 mM NaOH + 1 mM KOH + 1 mM RbOH + 1 mM CsOH.

Table 8. Alkali Metal Ion Concentrations of Li-Concentrated Solutions (10 mL) before and after the Treatment with 100 mg of R12(H)

		concentration/mM			
solution[a]	adsorption	Li	Na	K	pH
C	before	4.2×10^2	4.3	1.0	5.4
C	after	4.2×10^2	8.3×10^{-1} (81%)[b]	6.1×10^{-3} (99.4%)	2.6
D	before	4.3×10^2	4.3	1.0	12.6
D	after	4.3×10^2	7.8×10^{-2} (98%)	1.3×10^{-3} (99.9%)	11.1

[a] C: 420 mM LiCl + 4.3 mM NaCl + 1.0 mM KCl; D: 410 mM LiCl + 20 mM LiOH + 4.3 mM NaCl + 1.0 mM KCl. [b] Numbers in parentheses are removal rates.

and bare lithium ions may cause its high K_d value at pH around 7.

Removal of Minor Amounts of Na^+ and K^+ for Purification. From an applied stand point, the present exchanger can be used to purify a Li^+-containing solution by removal of minor amounts of Na^+ and K^+. Table 8 lists the results of the removal of Na^+ and K^+ from the two kinds of Li^+-concentrated solutions with different OH^- concentrations. In the case of 420 mM LiCl solution containing small amounts of NaCl and KCl, the lithium concentration did not show noticeable change after the treatment with R12(H), while the sodium and potassium concentrations decreased markedly, corresponding to removal rates of 81 and 99.4%, respectively. The removal of sodium and potassium is even more effective with a (LiCl + LiOH) solution at high pH, as the removal rates reach 98 and 99.9%, respectively, from a solution of 410 mM LiCl and 20 mM LiOH. These results indicate that the present sample holds great promise as an adsorbent for the selective removal of Na^+ and K^+ from a solution containing a concentrated lithium compound.

Conclusion

A novel inorganic ion exchanger, $(H_3O)_8Nb_{22}O_{59}$, can be developed by topotactic extraction of Rb^+ from $Rb_8Nb_{22}O_{59}$ via a H_3O^+/Rb^+ ion-exchange reaction in a HNO_3 solution. The obtained crystal has a hexagonal structure with almost the same lattice parameters ($a = 7.5104(2)$ and $c = 43.0780(8)$ Å) as the precursor $Rb_8Nb_{22}O_{59}$. It has an ion-sieve property depending on the size of pores formed in the lattice of the niobium oxide network. It is promising as an adsorbent for purification of lithium or cesium compound, owing to its selective adsorptive properties for minor K^+ and Na^+ impurities.

CM050835E